

Development of Cardanol-Based Polyol via Click Chemistry and Crosslinking with Melamine Formaldehyde Resin for Coating Applications

Kunal Wazarkar and Anagha Sabnis*

Department of Polymer and Surface Engineering, Institute of Chemical Technology, Nathalal Parekh Marg, Matunga (E), Mumbai 400019, India

Received July 13, 2017; Accepted August 03, 2017

ABSTRACT: The research work presented in this article deals with the synthesis of cardanol-based polyol and its curing with hexabutoxymethyl melamine (HBMM) for application in coatings. Cardanol-based polyol was prepared via thiol-ene click reaction using thioglycerol. Unsaturation present in the long chain of cardanol was successfully utilized to synthesize polyol via thiol-ene coupling. The reaction was carried out between cardanol and thioglycerol in the presence of Irgacure 184 (photoinitiator) and 1,8-Diazabicyclo[5.4.0]undec-7-ene (catalyst) under UV light for 12 h at 80 °C. After completion of the reaction, one mole of thioglycerol was successfully added across the double bond of a fatty chain of cardanol and confirmed by Fourier transform infrared spectroscopy (FTIR) and proton nuclear magnetic resonance spectroscopy and hydroxyl and iodine values were determined. Furthermore, the polyol thus prepared was cured with commercial HBMM in various proportions, such as 1:0.6, 1:0.8 and 1:1, on an equivalent basis. The coatings were then characterized for mechanical, chemical, optical, thermal and anticorrosive properties. It was observed that coatings exhibited excellent performance properties as compared to that of its acrylic counterpart.

KEYWORDS: CNSL, click chemistry, HBMM crosslinker, anticorrosive, sustainable

1 INTRODUCTION

Amino resins are a class of polymers that have been produced on a large scale for many years. Recently, amino resins have gained a broad spectrum of applications, including molding powder, textiles, adhesives, paper/pulpwood industries, varnish resin, fertilizers, crosslinker for alkyd, polyester and acrylic polyol resins, etc. [1–8]. Amongst these, melamine formaldehyde resin (MF) is one of the hardest and stiffest existing polymers that provides excellent scratch resistance and surface gloss as well as good performance properties. These MF resins are mainly used to improve the mechanical properties, moisture resistance, or fire resistance in many applications [9–11].

Biomaterials are rapidly gaining attention these days due to the fact that these materials are derived from renewable resources and are abundantly available in nature. With a little modification these materials

can be used to replace petroleum-based resources completely or partially. There are various materials which are used in the modern coating industry for a wide variety of applications, some of which are cashew nut shell liquid (CNSL), vegetable oils, fats, eugenol, citric, tartaric and itaconic acids, cellulose, starch, sucrose, sugar, lignin, etc. [12]. Amongst these, CNSL is abundantly available and can be easily modified to suit coating and other applications. It mainly contains phenolic compounds, viz., cardol, 2-methyl cardol, cardanol and anacardic acid [13]. Out of these, cardanol contains phenol group and C15 long aliphatic chain at the meta position, which makes it suitable for a number of reaction chemistries. The resultant products are then used in a number of industrial applications like resins, paints and coatings, adhesives, lacquers, and hybrid materials [14, 15].

Unsaturation in cardanol can be modified by using various chemistries, such as epoxidation, maleinization and thiol-ene click reaction, to introduce additional functionalities to help in improving the final properties of the polymer or coating. In 2001, Sharpless *et al.* described click reaction as a reaction wherein a weak sulphur hydrogen bond present in the

*Corresponding author: as.sabnis@ictmumbai.edu.in

thiol compounds can undergo various chemical reactions to produce a variety of useful monomers and oligomers. Moreover, the reaction is fast, forms low or no by-products and solvent medium is not required [16–22]. Due to such advantages, thiol-ene coupling has received a lot of attention recently.

The thiol-ene reaction proceeds as a typical radical chain process with initiation, propagation and termination steps [23–25]. However, various factors need to be considered while carrying out this reaction: a) The reactivity of alkenes varies significantly depending on the nature of C=C bond. For example, addition of thiols across terminal double bonds (eugenol, vinyl ethers, etc.) is much more efficient than that across the highly strained double bonds (norbornene, double bonds in vegetable oils, etc.). b) The reaction can be catalyzed by the addition of nucleophilic catalysts such as phosphines and amines, as it hinders the probability of polymerization of C=C containing compounds [26].

Thiol-ene reaction with biobased raw materials is an attractive, energy efficient and economical way of synthesizing a variety of products. Vegetable oils [27, 28], such as linseed oil [29–31], sunflower oil, soybean oil [32], castor oils [33], and grape seed oil [34], have been modified with thiol-ene reaction for various applications in the polymer industry [35]. The addition of thiols across double bonds is greatly affected by both structures of thiols and the nature of unsaturation (conjugated, non-conjugated, terminal, middle, etc.) [36]. Recently, cardanol-based polyols synthesized by thiol-ene coupling and polyurethane coatings have been prepared. The resultant coatings were evaluated for performance properties [37]. In our previous work, cardanol-based polyols were developed from an epoxy derivative of cardanol (NC-514) and tartaric acid followed by crosslinking with various concentrations of hexamethoxy methyl melamine (HMMM). The results were promising, as the coatings showed excellent mechanical, chemical, thermal and anticorrosion properties [38].

In the present work, a more convenient, easier method for the preparation of cardanol-based polyol was employed, viz., thiol-ene coupling. The thiol-ene process required comparatively less temperature than that of the conventional polycondensation process. Thus, controlling the reaction is much easier in the latter case. Furthermore, synthesized polyol was cured with commercial hexabutoxymethyl melamine (HBMM) in various concentrations (polyol:HBMM – 1:0.6, 1:0.8, 1:1 on equivalent basis) to prepare coatings. Moreover, the coatings were evaluated for performance properties, including mechanical, chemical, optical, anticorrosive and thermal. In addition, the effect of the crosslinker ratio on the final properties of the coatings was investigated.

2 MATERIALS

Cardanol (NC-700) was provided by Cardolite Specialty Chemicals Ltd., Mangalore, India. Thioglycerol, p-toluene sulfonic acid (p-TSA), 1,8-Diazabicycloundec-7-ene (DBU) and Irgacure 184 were purchased from SD Fine Chemicals, Mumbai, and were used as received. Commercial MF resin [(N, N, N', N', N'', N''-Hexakis(butoxymethyl)-1,3,5-triazine-2,4,6-triamine (HBMM); solids: 60%)] was provided by Shalimar Paints Ltd., Nashik, India. Commercial acrylic polyol (R-946; NVM-100%; Hydroxyl Value: 100–105 mg of KOH/g) was provided by Resins & Plastics Ltd., Mumbai, India.

3 EXPERIMENTAL

3.1 Synthesis of Cardanol-Based Polyol (Card-S-ol)

The reaction was carried out in a single-neck round-bottom flask fitted with water condenser. To obtain 1 mole addition of thioglycerol across any of the double bonds present in the cardanol molecule, reaction parameters were optimized to molar ratio of cardanol to thioglycerol 1:5, Irgacure 184 (1.5 wt% based on solids) and 1,8-Diazabicyclo[5.4.0]undec-7-ene (1 wt% based on solids). The flask was magnetically stirred for 12 h at 80 °C in the presence of UV light. After completion of the reaction, the mixture was washed with 1% aq NaOH solution followed by washings with lukewarm water to remove excess thioglycerol and traces of the catalyst. The product was dried over anhydrous sodium sulfate to give viscous dark maroon colored product with 91% yield. The product was characterized for hydroxyl value, FTIR, ¹H-NMR spectroscopy and gel permeation chromatography. Figure 1 shows a schematic representation of the preparation of Card-S-ol.

3.2 Surface Preparation of Mild Steel Panels

The mild steel substrates with dimensions 150 mm × 100 mm × 0.5 mm were first degreased with cleaner solution for 15 min. These substrates were further washed with tap water and dried. The substrates were then polished with Emery paper 80 and finally wiped with cotton dipped in acetone.

3.3 Coating Preparation

For curing of the formulation, the ratio of HBMM to Card-S-ol was varied on equivalent basis, such as

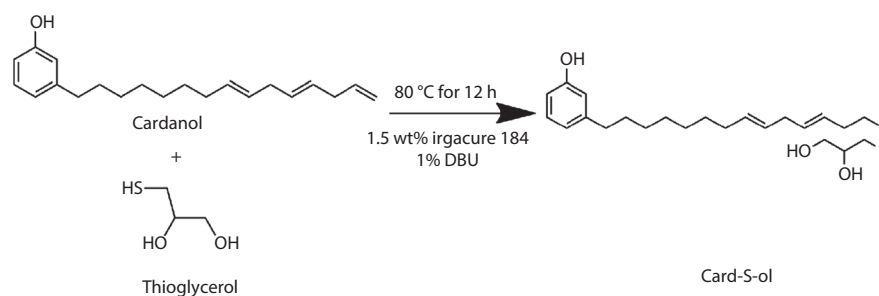


Figure 1 Schematic representation of synthesis of Card-S-ol.

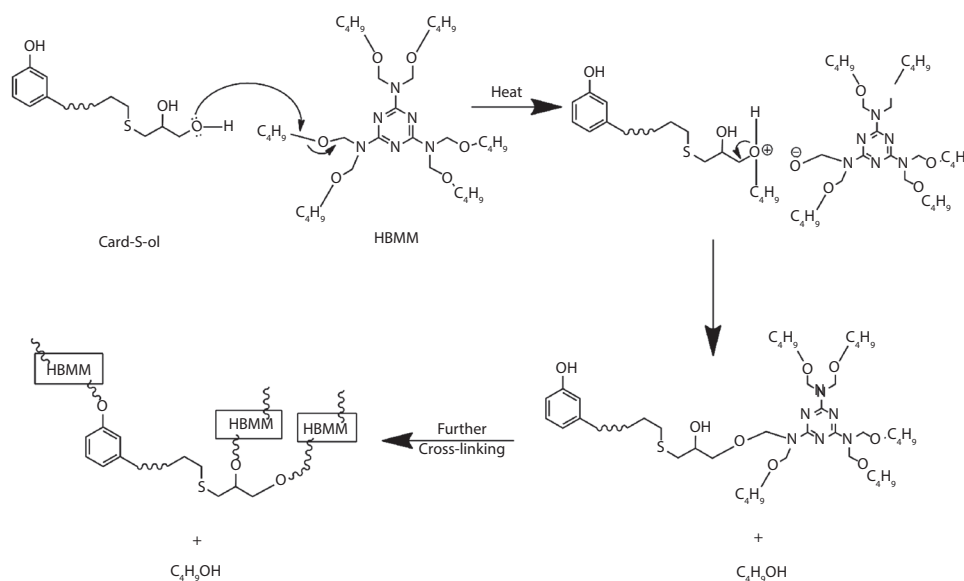


Figure 2 Crosslinking reaction of Card-S-ol with HBMM.

0.6:1, 0.8:1 and 1:1, and wt% are shown in the Table 1. In a similar manner, coatings with commercial acrylic polyol were also prepared for comparison purpose. The calculated amount of polyol and HBMM was mixed with xylene/butanol (70/30 on v/v) solvent mixture to attain application viscosity. Then, 3 wt% of total formulation p-toluene sulfonic acid was added as a catalyst. The mixture was applied on mild steel substrates by flow method and given a flash of f for 10–15 min before putting them in the oven. The substrates were then thermally cured at 150 °C for 30 min to get completely dried coating. The coated substrates were then evaluated for physical, mechanical, chemical, thermal and anticorrosive properties. Coatings based on Card-S-ol were represented by “SMF” followed by the amount of crosslinker and coatings based on acrylic polyol were represented by “AMF” followed by the amount of crosslinker. Figure 2 represents the curing mechanism of Card-S-ol-HBMM systems.

Table 1 Formulation of polyol-HBMM system.

Formulation (Card-S-ol:HBMM)	Card-S-ol (wt%)	HBMM (wt%)
1:0.6	67.8%	32.2%
1:0.8	61.2%	38.8%
1:1	55.8%	44.2%

4 CHARACTERIZATION

The hydroxyl number of the polyol prepared was evaluated by acetic anhydride-pyridine method. The hydroxyl values were calculated by the following equation:

$$\text{Hydroxyl Value} = \frac{56.1 \times (B - S) \times N}{w} \quad (1)$$

Here, N = Normality of alcoholic KOH solution; B = burette reading for the blank solution; S = burette

reading for sample analyzed; and W = weight of the sample analyzed.

Iodine value was determined according to ASTM D1959. The gel content (GC) was evaluated to determine the extent of crosslinking of coatings. The known weight of sample (w_0) was put into 20 ml THF for 24 h. After 24 h, the entire mixture was filtered and the contents on the filter paper were dried in an oven at 50 °C and weighed again (w_2). GC was then calculated using Equation 2.

$$\text{Gel content (\%)} = \frac{w_2 \times 100}{w_0} \quad (2)$$

To measure water absorption of coating films, sample with known weight was dipped in water at room temperature for 24 h. After 24 h of immersion, the sample was taken out and any drops of water left on the polymer surface were soaked with cotton. The sample was then weighed and the weight gain was then calculated from the difference in the weights of the sample before and after soaking in water according to Equation 3:

$$\text{Water absorption (\%)} = \frac{(W_{\text{after}} - W_{\text{before}}) \times 100}{W_{\text{before}}} \quad (3)$$

where W_{after} is the weight of the sample after dipping in water and W_{before} is the weight of the sample before dipping in water.

Applied coatings were tested for adhesion properties by cross-cut adhesion according to ASTM D3359B. A lattice pattern of cuts with equal spacing was made on the coating surface with the cross hatch cutter and commercial cellophane tape was applied over the lattice. The substrate was then examined for any loss of the squares from the lattice pattern. Pull-off adhesion strength of coatings was evaluated by the portable adhesion tester as per ASTM D4541. Pencil and scratch hardness of the coating were measured on a hardness tester according to ASTM D3363 and IS 104 respectively. Flexibility and load distribution property of the coating were determined by conical mandrel and impact tester as per ASTM D522 and ASTM D2794 respectively. Impact resistance was measured on the impact tester with a maximum height of 23.6 inches and a load of 3 lbs. The chemical resistance of the coated panels was evaluated by acid and alkali as well as a water immersion method according to ASTM D1308 and ASTM D870 respectively. The degree of adhesion and visual inspection of blister and cracks was evaluated for coated panels after immersion of 24 h. The solvent resistance was measured by rub test. Completely cured coatings were tested for their

hydrolytic stability as per ASTM B1308. The coated panel was immersed in boiling water for 4 h and was evaluated for loss of adhesion and blister formation, if any.

5 INSTRUMENTATION

The FTIR spectra were recorded on Bruker instruments in the wavelength range of 4000–400 cm^{-1} at 24 scans and 2 cm^{-1} of resolution. The NMR spectra were recorded on a Mercury Plus NMR spectrometer (400 MHz, Varian, USA). CDCl_3 was used as solvent for all the samples evaluated. The chemical shifts in the discussion are reported in parts per million. The number average (M_n) molecular weight and molecular weight distribution was determined by gel permeation chromatography (GPC) (Agilent 1100 series). The sample was dissolved in tetrahydrofuran and placed in an Agilent 1100 series instrument, consisting of a refractive index (RI) detector and Agilent PL gel 10 μm column. The glass transition temperature measurement was performed by differential scanning calorimetry (DSC) on DSC Q-100 equipment (TA Instruments, USA). The samples were evaluated in two heat cycles of 40 to 100 °C and –20 to 100 °C at a heating rate of 10 °C/min under nitrogen atmosphere. The thermogravimetric analysis (TGA) of coating samples was performed on a DSC Q-100 instrument under nitrogen atmosphere in the temperature range of 40–600 °C at a heating rate of 10 °C/min. The wide angle X-ray diffraction (XRD) patterns were evaluated using a Rigaku Miniflex X-ray diffractometer (Rigaku Europe, Germany). The 2θ diffraction was scanned from 2° to 80° at an interval of 0.05°. The percentage crystallinity was calculated from the integral of crystalline area and integral of total area. The anticorrosive performance of the coated panels was evaluated by electrochemical impedance spectroscopy (EIS) and Tafel analysis. For this purpose, a VersaSTAT 3 instrument (AMETEK, Princeton Applied Research, Oak Ridge, TN) was used and all electrochemical measurements were obtained at room temperature (30 °C) in 3.5% NaCl solution. The test system consisted of three electrode cells, in which a calomel electrode, a platinum electrode and a coated panel were used as reference, counter and working electrode respectively. The exposed area of the coated panels to the NaCl solution was 7 cm^2 in all cases. Corrosion parameters of the coatings were evaluated as reported in [39].

6 RESULTS AND DISCUSSIONS

Synthesized polyol was confirmed by chemical (hydroxyl value and iodine value) as well as

spectroscopic analysis (FTIR, $^1\text{H-NMR}$ and GPC). Hydroxyl value of the product was practically evaluated by titration method and observed to be 388.5 mg of KOH/g of sample, which was closer to the theoretical hydroxyl value, viz., 408.5 mg of KOH/g of sample. Moreover, the practical iodine value of the product was observed to be reduced to 107.4 g of iodine per 100 g of sample, which was closer to the theoretical iodine value 110.8 g of iodine per 100 g of sample.

6.1 FTIR Spectroscopy

Functional group analysis was done using FTIR spectroscopy and is shown in Figure 3. Major transmission bands observed at 3331 cm^{-1} and 1028 cm^{-1} confirmed the presence of hydroxyl group and $-\text{C-S-}$ linkage respectively. Moreover, absence of peak at 2557 cm^{-1} indicated successful utilization of thioglycerol across double bond of cardanol [25]. In addition, peak at 1588 cm^{-1} confirmed the presence of $-\text{C}=\text{C}$ aromatic linkage in cardanol. Peaks at 2852 and 2923 cm^{-1} indicated the methylene and terminal methyl group in cardanol aliphatic chain.

6.2 $^1\text{H-NMR}$ Spectroscopy

The chemical structure of Card-S-ol was confirmed by $^1\text{H-NMR}$ spectroscopy, as represented in Figure 5; for

comparison purpose, $^1\text{H-NMR}$ of cardanol was also provided (as shown in Figure 4). As can be seen from Figure 5, the peak at 0.8 ppm could be attributed to the terminal methyl group of alkyl chain in cardanol. Furthermore, peaks ranging from 4.95–5.8 ppm could be ascribed to the protons of carbon-carbon double bonds in the long chain of cardanol. As can be seen from both the figures, terminal proton shifts disappeared in Card-S-ol structure and new protons generated in the range of 3.4–3.9 ppm, which could be due to the protons arising from hydroxyl groups of thioglycerol and methylene protons adjacent to them [37]. Other common peaks observed at 2.62, 2.40, 2.18, 1.59 and 1.28 ppm could be attributed to the protons attached to methylene groups of aliphatic chain.

Griesbaum stated that the addition of thiol to symmetrical double bonds is slower as compared to the unsymmetrical ones (terminal double bonds). In the case of symmetric alkenes, steric hindrance as well as isomerization of double bonds are responsible for lowering the rate of thiol addition. It was observed that the intermediate alkyl radical formed between the two isomeric forms have a rather short lifetime and low resonance stability, which hampers its reaction with thiol. Therefore, the thiol-ene addition takes place across only the terminal single bond of cardanol [40].

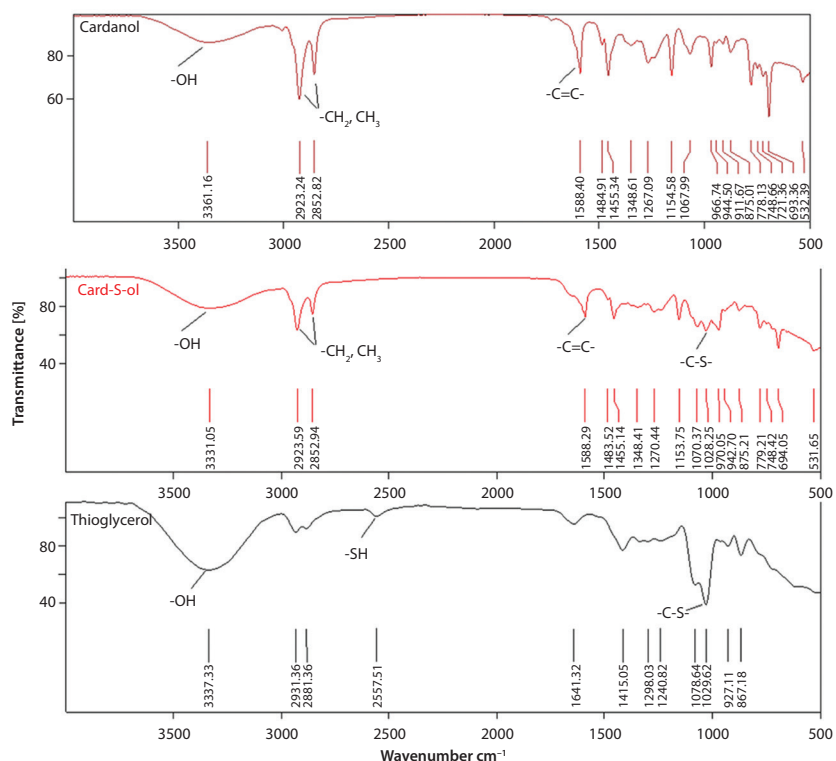


Figure 3 FTIR spectra of Card-S-ol.

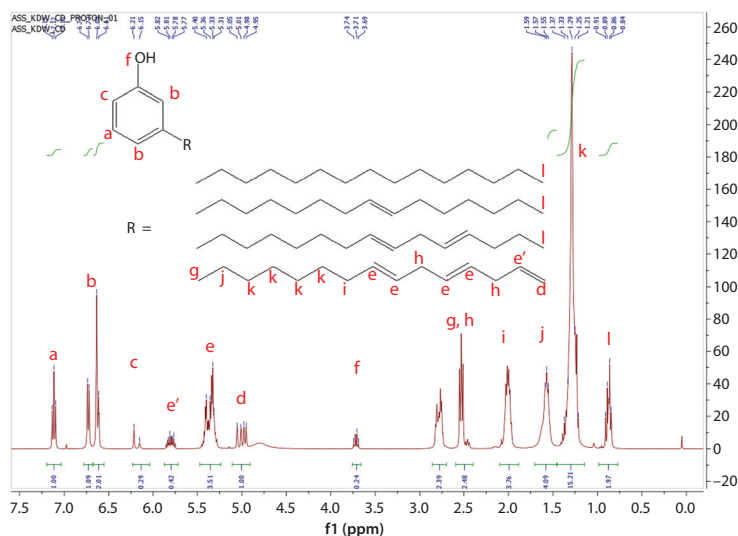


Figure 4 $^1\text{H-NMR}$ of cardanol.

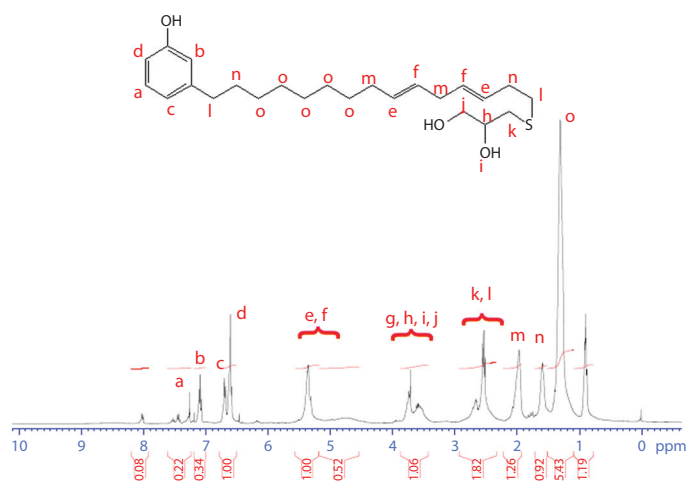


Figure 5 $^1\text{H-NMR}$ of Card-S-ol.

6.3 Gel Permeation Chromatography

Analysis of Card-S-ol was carried out by GPC to determine its molecular weight and the chromatograph is shown in Figure 6.

As can be seen from Table 2, molecular weight of Card-S-ol as evaluated from GPC was observed to be closer to the theoretical molecular weight. Overall, it can be concluded that one mole of thioglycerol was successfully added across the cardanol double bond through thiol-ene addition.

6.4 Coating Properties

The objective of this work is to investigate the effect of MF crosslinker on the final properties of the coating.

As the concentration of HBMM varies in the formulation, performance properties vary accordingly. HBMM has six functionalities and therefore provides hard and rigid structure to the final polymer and it is expected that hardness and rigidity of coatings will increase with an increase in concentration of HBMM. Figure 7 shows the coating films and Card-S-ol product.

6.4.1 Mechanical Properties

All the coatings were applied onto the mild steel panels and allowed to cure at 150 °C for 25–30 minutes. It was observed that dry film thickness of all the coatings was in the range of 50–70 microns. Completely cured coatings were evaluated for mechanical, chemical, optical, anticorrosive and thermal properties. Mechanical

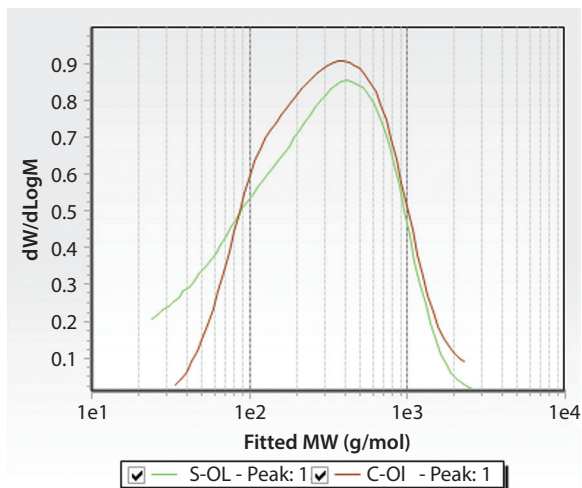


Figure 6 GPC chromatograph of Card-S-ol.

Table 2 GPC analysis of Card-S-ol.

Compound	Theoretical molecular weight	Practical Mn (g/mol)	Polydispersity index (PDI)
Cardanol	303	297	2.09
Card-S-ol	412	404	1.98

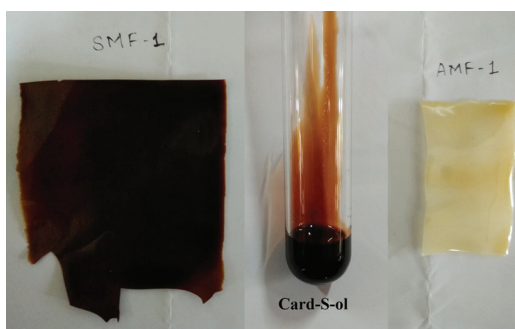


Figure 7 Card-S-ol and coating films cured with HBMM.

properties of the coatings are tabulated in Table 3. Extent of crosslinking of coatings was evaluated by determining the gel content. Gel content values gradually increased with an increase in concentration of crosslinker in Card-S-ol as well as acrylic polyol-based coatings. Concentration of crosslinker directly affected the gel content values, thereby increasing the crosslink density of coating films. All the coatings exhibited more than 91% of gel content. Similarly, the gloss of the coating depends on the crosslink density and inherent structure of the polymer backbone. As expected, gloss values increased with an increase in concentration of

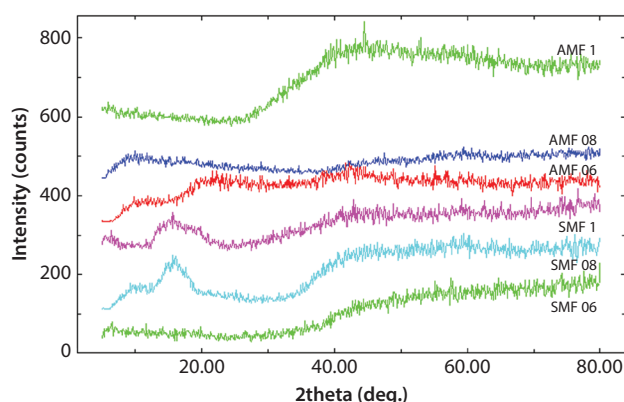
crosslinker. Comparatively, coatings based on acrylic polyol exhibited slightly higher gloss values as compared to that of the Card-S-ol-based coatings. Higher gloss values could be attributed to the presence of acrylic moiety in the structure. Furthermore, adhesion of all the coatings was observed to be excellent, as indicated by pull-off values of 1–1.2 MPa and 5B rating. Polar ether linkages generated after crosslinking could be responsible for the excellent adhesion of the coatings. Hardness of the coating is a measure of crosslink density and presence of hard moieties in the structure. With the decrease in concentration of Card-S-ol, concentration of flexible moieties present in the polymer backbone was reduced. In addition, with the increase in concentration of crosslinker, crosslink density increased, thereby increasing hardness values. Thus, SMF-1 exhibited the highest pencil and scratch hardness values among the series. Although no change in pencil hardness values was observed for both types of coating, scratch hardness offered by Card-S-ol-based coatings were much higher compared to its acrylic counterpart. On the contrary, as mentioned earlier, an increase in concentration of Card-S-ol increased the amount of flexible moieties that helped in the improvement of load distribution property, as observed by impact resistance and flexibility values. In other words, with the increase in the amount of crosslinker the load distribution property of coating was reduced, making it brittle and susceptible to breaking under impact. Hence, AMF-1 exhibited poor impact resistance and flexibility among the series. Comparatively, SMF-1 showed slightly better load distribution properties, as the presence of long aliphatic chain in Card-S-ol might be responsible for distributing the energy of impact uniformly over the surface. Water absorption of coatings was observed to be high (around 2.5%–3.5%). Curing of HBMM with polyols resulted in polar ether linkages which allow easy absorption of water, thus increasing water absorption of the coating films. Acrylic coatings exhibited higher water absorption values as compared to their Card-S-ol counterpart. This could be attributed to the presence of aromatic ring and hydrophobic long chain in the Card-S-ol, which managed to reduce the water absorption values below 3%.

6.4.2 X-ray Diffraction (XRD) Analysis

To evaluate percent crystallinity in the coatings, XRD analysis was performed and the diffractograms are shown in Figure 8. Most of the thermoset systems have an amorphous nature, as shown by broad peaks in the diffractograms. Similar results were observed in the case of Card-S-ol as well as acrylic systems. It was observed that the percent crystallinity was reduced

Table 3 Mechanical properties of commercial and Card-S-ol-based coatings.

Characterization	SMF-0.6	SMF-0.8	SMF-1	AMF-0.6	AMF-0.8	AMF-1
Gloss@60°	90–95	100–105	105–110	95–100	105–115	110–120
Gel content (%)	92.36	94.21	96.72	91.25	91.87	93.54
Adhesion	5B	5B	5B	5B	5B	5B
Pull-off adhesion (MPa)	1.04	1.20	1.16	1.09	1.01	1.18
Pencil hardness	4H	6H	6H	5H	6H	6H
Scratch hardness (kg)	2.3	2.5	2.8	2.1	2.4	2.5
Impact resistance (lbs/inch) Intrusion	70.86	70.86	70.86	70.86	64.96	59.05
Extrusion	70.86	64.96	59.06	70.86	47.24	23.62
Flexibility	0	2	4	0	5	10
Water absorption (%)	2.9	2.6	1.8	3.7	3.1	2.8

**Figure 8** XRD diffractograms of commercial and Card-S-ol-based coatings.

with an increase in the concentration of Card-S-ol. It could be possible that with higher concentration of Card-S-ol, the quantity of crosslinker added might not be sufficient to achieve complete curing, causing lower crystallinity in the films. Therefore, SMF-1 exhibited the highest percent crystallinity amongst the series (as shown in Table 4). Comparatively, all SMF coating films exhibited higher percent crystallinity as compared to their acrylic counterpart. The trifunctional nature of Card-S-ol might be responsible for higher values of percent crystallinity.

6.4.3 Chemical Properties

The chemical resistance test was carried out by dipping the coated panels in 5% HCl and 5% NaOH solutions for 24 h and observed for film defects, if any (see Table 5). It was observed that all the coatings exhibited excellent resistance to alkali as no film defects, such as loss of gloss, etching of film, softening of film, etc.,

Table 4 Percent crystallinity of films.

Coatings	% crystallinity
AMF-0.6	1.23
AMF-0.8	4.60
AMF-1	7.71
SMF-0.6	2.02
SMF-0.8	5.38
SMF-1	9.29

were observed on coated panels. However, a slight loss of gloss was observed when immersed in an acid solution for 24 h. Presence of free nitrogen in HBMM may form quaternary salts with acid component, causing reduction in gloss of coatings. Hydrolytic stability evaluated by dipping the coated panels in boiling water for 4 h caused etching of coating films. Solvent resistance was evaluated by a solvent double rub method using methyl ethyl ketone (MEK) and xylene solvents. The coatings showed excellent resistance to xylene and methyl ethyl ketone as no ill effects, such as loss of gloss, blushing, blistering or etching of film, were observed on the coated panels even after 200 rubs each of xylene and methyl ethyl ketone.

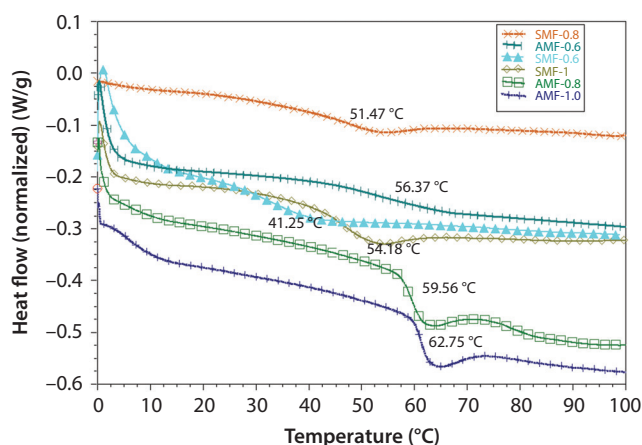
6.4.4 Thermal Properties

6.4.4.1 Glass Transition Temperature

In order to determine the glass transition temperature (T_g) of coating films as well as curing temperature of the formulations, DSC thermograms of all the coatings were performed, which are shown in Figure 9 and Figure 10 respectively. It is obvious that with the increase in crosslinker concentration crosslink density

Table 5 Chemical resistance of commercial and Card-S-ol-based coatings.

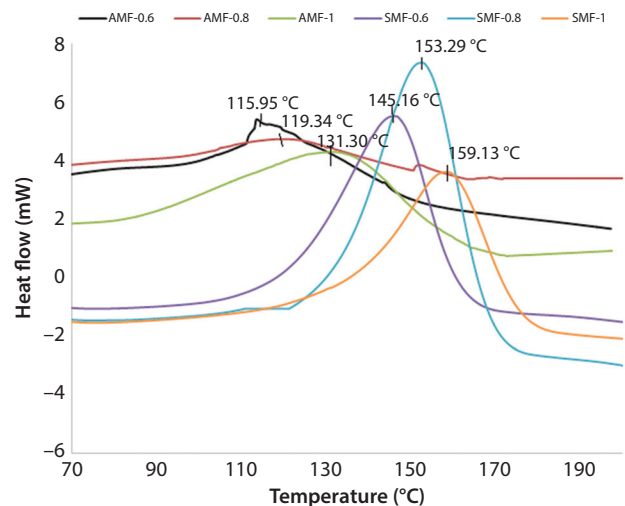
Coatings	Acid resistance	Alkali resistance	Hydrolytic stability	Solvent resistance	
				MEK	Xylene
SMF-0.6	Loss of gloss	Pass	Etching of film	>200	>200
SMF-0.8	Loss of gloss	Pass	Etching of film	>200	>200
SMF-1	Loss of gloss	Pass	Etching of film	>200	>200
AMF-0.6	Loss of gloss	Pass	Etching of film	>200	>200
AMF-0.6	Loss of gloss	Pass	Etching of film	>200	>200
AMF-1	Loss of gloss	Pass	Etching of film	>200	>200

**Figure 9** Glass transition temperature of acrylic and Card-S-ol-based coatings.

increases, thereby increasing the glass transition temperature of coatings. Consequently, as the concentration of Card-S-ol was reduced, the concentration of flexible aliphatic chains was also reduced. This reduction lowered the segmental motion in polymer chains and resulted in higher T_g values. Similar behavior was observed in all cases of coatings. However, T_g values exhibited by AMF coatings were rather high as compared to corresponding Card-S-ol coatings. As can be seen from Figure 9, the highest T_g was observed in the case of SMF-1 followed by SMF-0.8, and the least for SMF-0.6. Therefore, in the case of SMF coatings, T_g values ranged from 41–54 °C, while in the case of acrylic-PU coating it ranged from 56–62 °C.

6.4.4.2 Curing Temperature

The curing temperature of all compositions was investigated using DSC analysis and is shown in Figure 10. All the formulations were mixed in stoichiometric proportion and heated from -15 °C to 180 °C at a heating rate of 10 °C/min under nitrogen atmosphere. As expected, the curing temperatures of all formulations

**Figure 10** Curing temperatures of coatings at heating rate of 10 °C/min.

were higher than 100 °C. In comparison, AMF coatings exhibited lower curing temperatures than that of SMF coatings. Moreover, with the increase in concentration of crosslinker, curing temperature increased in both types of coatings. As can be seen from Figure 10, SMF-1 exhibited the highest curing temperature of 159 °C and that of AMF-1 was 131 °C. This could be explained by the hydroxyl content in respective polyols.

The hydroxyl equivalent of Card-S-ol is lower as compared to acrylic polyol, therefore the comparative amount of HBMM crosslinker required for SMF coatings is higher than that of AMF coatings and hence higher curing exotherms were observed for SMF coatings.

6.4.5 Anticorrosive Properties

Anticorrosive properties of coatings were evaluated using electron impedance spectroscopy (EIS) and DC polarization analysis.

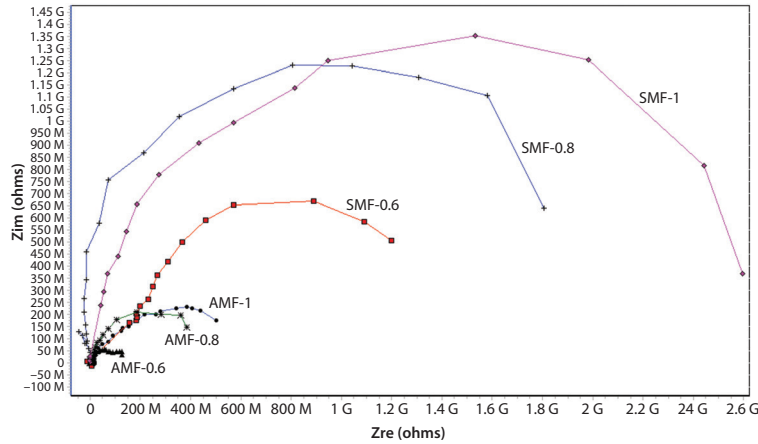


Figure 11 Nyquist plot of commercial and Card-S-ol-based coatings.

Table 6 EIS parameters of commercial and Card-S-ol-based coatings.

Coatings	Coating resistance (ohm/cm ²)	Coating capacitance (F/cm ²)
AMF-0.6	1.087E+05	1.476E-09
AMF-0.8	6.851E+05	9.947E-10
AMF-1	1.07E+08	1.73E-10
SMF-0.6	2.22E+08	2.12E-10
SMF-0.8	4.10E+08	1.23E-10
SMF-1	2.61E+09	2.436E-13

Nyquist plots of coatings are presented in Figure 11. It was observed that coating resistance was improved to increase concentration of crosslinker. The increase in crosslinker concentration imparted hard and rigid structure to the coatings, which was responsible for increasing corrosion resistance. In addition, SMF coatings showed superior corrosion resistance compared to corresponding AMF coatings. Superior impedance values could be related to a number of factors such as an aromatic ring of Card-S-ol, presence of sulfur atom and the trifunctional nature of polyol. Therefore, SMF-1 showed excellent corrosion resistance amongst the series.

Moreover, coating capacitance values decreased with an increase in concentration of crosslinker. Capacitance values are related to water diffusion through the coating; the greater the water diffusion, the greater the coating capacitance and vice versa. SMF coatings showed comparatively lower values of coating capacitance than that of AMF coatings (see Table 6). It was also evident from water absorption values that SMF-1 had excellent impermeability to water. Lower water diffusion values of SMF coatings suggested that SMF coatings were highly impermeable to

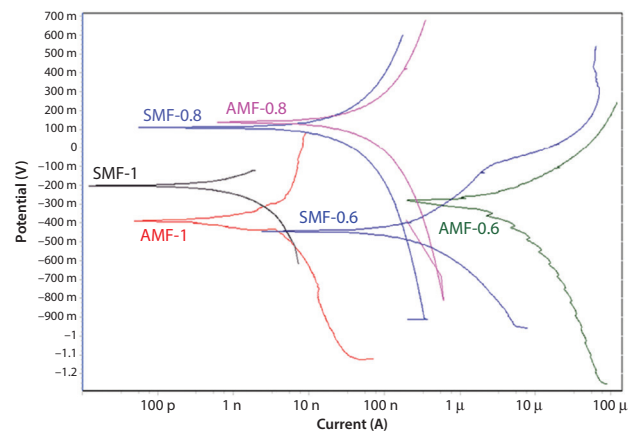


Figure 12 Tafel plots of commercial and Card-S-ol-based coatings.

Table 7 Tafel parameters of commercial and Card-S-ol-based coatings.

Coatings	Potential (mV)	Current (A)	Corrosion rate (mppy)
AMF-0.6	-276.5	3.02E-06	5.03E-02
AMF-0.8	137.2	2.68E-08	4.45E-05
AMF-1	-397.5	2.25E-09	3.74E-06
SMF-0.6	-446.3	2.86E-07	4.76E-04
SMF-0.8	104.8	9.84E-09	1.64E-05
SMF-1	-201.3	0.61E-09	1.01E-06

water and thus exhibited excellent corrosion protection to the metal substrate.

Similar results were also obtained in Tafel analysis. As shown in Figure 12, SMF coatings exhibited higher potential values, lower current values and lower corrosion rates (as shown in Table 7) when compared

with AMF coatings. Moreover, with an increase in crosslinker concentration there is a rise in rigidity and compactness of coating film, which provided an excellent barrier for corroding species. Therefore, SMF-1 provided excellent corrosion protection amongst the series while AMF-0.6 provided the least corrosion resistance.

7 CONCLUSION

Sulfur-containing polyol based on cardanol was successfully prepared via click chemistry. Coatings were cured with various concentrations of hexabutoxy methyl melamine to study the effect on final performance properties. It was observed that with an increase in concentration of the hexabutoxy methyl melamine, hardness, adhesion, impermeability to water and gloss of coatings improved, while reducing flexibility and impact resistance. A reduction in glass transition temperature was observed with the increase in concentration of Card-S-ol. The presence of flexible aliphatic chain present in the structure would likely impart plasticizing effect and reduce the glass transition temperature. EIS and DC polarization studies revealed that coatings based on Card-S-ol exhibited superior corrosion resistance, lower capacitance, corrosion current and corrosion rates as compared to that of their acrylic counterpart.

ACKNOWLEDGMENT

The authors are grateful to Cardolite Specialty Chemicals, India, for providing NC-700 sample. The authors are also thankful to Shalimar Paints Ltd. and Resins & Plastics Ltd., India, for providing hexabutoxymethyl melamine and acrylic polyol (R-946) respectively. The authors would like to thank UGC-BSR-[F.25-1/2014-15 (BSR)/No. F.7-314/2010(BSR)] for funding the project.

REFERENCES

1. S. Jahromi, Storage stability of melamine-formaldehyde resin solutions: The mechanism of instability. *Macromol. Chem. Phys.* **200**, 2230–2239 (1999).
2. S. Jahromi, The storage stability of melamine formaldehyde resin solutions: III. Storage at elevated temperatures. *Polymer* **40**, 5103–5109 (1999).
3. S. Jahromi, V. Litvinov, and E. Gelade, Physical gelation of melamine formaldehyde resin solutions. II. A combined light-scattering and low-resolution relaxation proton NMR study. *J. Polym. Sci. Part B: Polym. Phys.* **37**, 3307–3318 (1999).

4. C. Devallencourt, J.M. Saiter, and D. Capitaine, Reactions between melamine formaldehyde resin and cellulose: Influence of pH. *J. Appl. Polym. Sci.* **78**, 1884–1896 (2000).
5. M. Singh and V. Kumar, Preparation and characterization of melamine– formaldehyde–polyvinyl pyrrolidone polymer resin for better industrial uses over melamine resins. *J. Appl. Polym. Sci.* **114**, 1870–1878 (2009).
6. N. Miyauchi, M. Kusahara, T. Motomura, and M. Akashi, Acrylic nonaqueous dispersion using butylated melamine-formaldehyde resin as dispersant. *J. Appl. Polym. Sci.* **37**, 915–923 (1989).
7. Y. Motoyama and K. Uchida, Preparation of sec-butanol-modified melamine-formaldehyde resin varnish. *J. Appl. Polym. Sci.* **11**, 1251–1257 (1967).
8. K. Dietrich, H. Herma, R. Nastke, E. Bonatz, and W. Teige, Amino resin microcapsules literature and patent review. *Acta Polym.* **40**, 243–251 (1989).
9. B.D. Park and H.W. Jeong, Cure kinetics of melamine– formaldehyde resin/clay/cellulose nanocomposites. *J. Ind. Eng. Chem.* **16**, 375–379 (2010).
10. K. Dietrich, E. Bonatz, H. Geistlinger, H. Herma, R. Nastke, H. Jpurz, M. Schlawne, and W. Teige, Amino resin microcapsules II. Preparation and morphology. *Acta Polym.* **40**, 325–331 (1989).
11. K. Dietrich, E. Bonatz, R. Nastke, H. Herma, M. Walter, and W. Teige, Amino resin microcapsules IV. Surface tension of the resins and mechanism of capsule formation. *Acta Polym.* **11**, 91–95 (1990).
12. D. Balgude and A. Sabnis, CNSL: An environment friendly alternative for the modern coating industry. *J. Coat. Technol. Res.* **11**, 169–183 (2014).
13. M.C. Lubi and E.T. Thachil, Cashew nut shell liquid (CNSL) – A versatile monomer for polymer synthesis. *Des. Monomers Polym.* **3**, 123–153 (2000).
14. D. Balgude, K. Konge, and A. Sabnis, Synthesis and characterization of sol–gel derived CNSL based hybrid anti-corrosive coatings. *J. Sol-Gel Sci. Technol.* **69**, 155–165 (2014).
15. M. Kathalewar, A. Sabnis, and D. D’Mello, Isocyanate free polyurethanes from new CNSL based bis-cyclic carbonate and its application in coatings. *Eur. Polym. J.* **57**, 99–108 (2015).
16. D. Zhang, C. Liu, S. Chen, J. Zhang, J. Cheng, and M. Miao, Highly efficient preparation of hyperbranched epoxy resins by UV-initiated thiol-ene click reaction. *Prog. Org. Coat.* **101**, 178–185 (2016).
17. M. Sangermano, I. Roppolo, R. Acosta Ortiz, A. Gabriela, N. Tovar, A. Valdez, and M. Duarte, Interpenetrated hybrid thiol-ene/epoxy UV-cured network with enhanced impact resistance. *Prog. Org. Coat.* **78**, 244–248 (2015).
18. K. Aoki, R. Imanishi, and M. Yamad, Novel dendritic polyenes for application to tailor-made thiol-ene photopolymers with excellent UV-curing performance. *Prog. Org. Coat.* **100**, 105–110 (2016).
19. H.C. Kolb, M.G. Finn, and K.B. Sharpless, Click chemistry: Diverse chemical function from a few good reactions. *Angew. Chem. Int. Ed. Engl.* **40**, 2004–2021 (2001).
20. A.C. Pauly and F. Lena, Incorporating amino acid sequences into the backbone chain of polymers through thiol-ene chemistry. *Polymer* **72**, 378–381 (2015).

21. M. Podgórski, E. Becka, M. Claudino, A. Flores, P.K. Shah, J.W. Stansbury, and C.N. Bowman, Ester-free thiol-ene dental restoratives—Part A: Resin development. *Dent. Mater.* **31**, 1255–1262 (2015).
22. J. Samuelsson, M. Johansson, and T. Brinck, Thiol-ene coupling reaction of fatty acid monomers. *J. Polym. Sci. Part A: Polym. Chem.* **42**, 6346–6352 (2004).
23. C. Hoyle, T. Lee, and T. Roper, Thiol-enes: Chemistry of the past with promise of the future. *J. Polym. Sci. Part A: Polym. Chem.* **42**, 5301–5338 (2004).
24. C. Hoyle, A. Lowe, C. Bowman, Thio-click chemistry: A multifaced toolbox for small molecule and polymer synthesis. *Chem. Soc. Rev.* **39**, 1355–1387 (2010).
25. D. Guzman, X. Ramis, X. Francos, and A. Serra, Preparation of click thiol-ene/thiol-epoxy thermosets by controlled photo/thermal dual curing sequence. *RSC Adv.* **5**, 101623–101633 (2015).
26. Y. Duo, Y. Ping, D. Fang, S. Jin, J. Wa, G. Mou, Y. Yu, L. Yang, and L. Chin, Chemically bonded polyacrylamide via thiol-ene click chemistry as separation materials for hydrophilic interaction liquid chromatography. *J. Anal. Chem.* **43**, 1439–1444 (2015).
27. P. Alagi, Y.J. Choi, J. Seog, and S.C. Hong, Efficient and quantitative chemical transformation of vegetable oils to polyols through a thiol-ene reaction for thermoplastic polyurethanes. *Ind. Crops Prod.* **87**, 78–88 (2016).
28. C. Fu, Z. Zheng, Z. Yang, Y. Chen, and L. Shen, A fully bio-based waterborne polyurethane dispersion from vegetable oils: From synthesis of precursors by thiol-ene reaction to study of final material. *Prog. Org. Coat.* **77**, 53–60 (2014).
29. A.B. Lowe, Thiol-ene click reactions and recent applications in polymer and materials synthesis: A first update. *Polym. Chem.* **5**, 4820–4870 (2014).
30. Y.H. Zhao, D. Vulug, L. Lecamp, and F. Burel, A rapid, eco- and environmental friendly alternative to oil oxidation for the preparation of fatty coatings using photoinitiated thiol-ene chemistry. *Prog. Org. Coat.* **101**, 216–224 (2016).
31. T. Hayashi, A. Kazlauciuonas, and P.D. Thornton, Dye conjugation to linseed oil by highly-effective thiol-ene coupling and subsequent esterification reactions. *Dyes Pigm.* **123**, 304–316 (2015).
32. A.B. Lowe, Thiol-yne click/coupling chemistry and recent applications in polymer and materials synthesis and modification. *Polymer* **55**, 5517–5549 (2014).
33. M. He, S. Jiang, R. Xu, J. Yang, Z. Zeng, and G. Chen, Facile functionalization of soybean oil by thiol-ene photo-click reaction for the synthesis of polyfunctional acrylate. *Prog. Org. Coat.* **77**, 868–871 (2014).
34. G. Chen, X. Guan, R. Xu, J. Tian, M. He, W. Shen, and J. Yang, Synthesis and characterization of UV-curable castor oil-based polyfunctional polyurethane acrylate via photo-click chemistry and isocyanate polyurethane reaction. *Prog. Org. Coat.* **93**, 11–16 (2016).
35. M. Stemmelen, F. Pessel, V. Lapinte, S. Caillol, J.-P. Habas, and J.-J. Robin, A fully biobased epoxy resin from vegetable oils: From the synthesis of the precursors by thiol-ene reaction to the study of the final material. *J. Polym. Sci. Part A: Polym. Chem.* **49**, 2434–2444 (2011).
36. O. Türünç and M. Meier, The thiol-ene (click) reaction for the synthesis of plant oil derived polymers. *Eur. J. Lipid Sci. Technol.* **115**, 41–54 (2012).
37. C. Fu, J. Liu, H. Xia, and L. Shen, Effect of structure on the properties of polyurethanes based on aromatic cardanol-based polyols prepared by thiol-ene coupling. *Prog. Org. Coat.* **83**, 19–25 (2015).
38. D. Balgude, A. Sabnis, and S. Ghosh, Designing of cardanol based polyol and its curing kinetics with melamine formaldehyde resin. *Des. Monomers Polym.* **20**, 177–189 (2017).
39. K. Wazarkar, M. Kathalewar, and A. Sabnis, High performance polyurea coatings based on cardanol. *Prog. Org. Coat.* **106**, 96–110 (2017).
40. K. Griesbaum, Problems and possibilities of the free-radical addition of thiols to unsaturated compounds. *Angew. Chem. Int. Ed.* **9**, 273–287 (1970).